A new growth process for crystalline ultra-thin layers of conjugated oligomers used in field-effect transistor applications

S. RENKERT[a,b], S. FALL, S. MOTAMEN[b], Th. JARROSSON[d], F. SEREIN-SPIRAU[d], T. HEISER[c] L. SIMON[a], G. REITER[b], J.L. BUBENDORFF[a]

[a] Université de Strasbourg (UdS)-Université de Haute Alsace (UHA), Institut de Science des Matériaux de Mulhouse (IS2M), UMR 7361-CNRS, 3b rue Alfred Werner, 68093 Mulhouse, France.
[b] Physikalisches Institut, Albert-Ludwigs-Universität Freiburg i.Br., Hermann-Herderstraße 3, 79104 Freiburg, Germany.
[c] Université de Strasbourg (UdS), ICube UMR 7357, Laboratoire des sciences de l'ingénieur, de l'informatique et de l'imagerie, 300 bd Sébastien Brant - CS 10413 - 67412 Illkirch, France.
[d] Institut Charles Gerhardt de Montpellier, UMR 5353-CNRS, Université de Montpellier, Equipe Architectures Moléculaires et Matériaux Nanostructurés, Ecole Nationale Supérieure de Chimie de Montpellier, 8 rue de l'Ecole Normale, 34296 Montpellier cedex 05, France.

Abstract:

Most organic semiconductor materials dewet on silicon wafers with thermal oxide layers. While Si-wafers represent convenient substrates for building a field effect transistor (FET), dewetting largely destroys the possibility for obtaining a compact and continuous crystalline thin organic semiconductor film and thus limits the mobility in these systems. Using oligothiophenes, we present an approach where the initial dewetting process can be turned into an advantage for generating very thin but large crystalline domains of a size up to the millimetres with all molecules sharing a single orientation. Our approach can be easily extended to other molecules, which have strongly differing growth velocities in the various directions of the crystal, for example due to directional π-stacking interactions. FETs devices based on such large crystalline domains showed charge carrier mobilities that were two orders of magnitude higher compared to non-crystallized films.

Corresponding author.

E-mail address: jean-luc.bubendorff@uha.fr (J.L. Bubendorff)

Introduction

Organic semiconductors represent a key component in organic electronics and often determine the performance of a device. In the last three decades, they have been integrated in various applications, ranging from basic solar cells [1, 2], organic solar cells within textiles, flexible displays [3] to chemical sensors acting as electrical noses [4, 5] that can detect and distinguish traces of various molecules in the air. Research on organic semiconductors became an active field for various reasons beyond scientific curiosity. Compared to silicon-based semiconductors, manufacturing costs are considerably lower. The resulting devices are mechanically much more flexible, especially when using flexible substrates. Employing roll-to-roll printing methods [6] allow fabricating for example solar cells on various substrates, increasing the range of implementation of such devices. Electro-optical properties can be versatile such as tuneable band gaps. In addition, effects like chemical sensing of target molecules in a lock-and-key principle are correlated in a clear and unique way to the chemical structure of the molecules forming the organic semiconductor layer. Even small changes in the chemical structure of a molecule can lead to drastic changes in macroscopic material properties [7]. The almost unlimited number of chemical modifications allows for a large variability in materials properties, most of which still await their discovery [7]. Today, field effect transistors, light emitting diodes and solar cells based on organic semiconductors are available commercially. Many possibilities for new applications have been revealed thanks to the exceptional properties of these materials [8]. For example, fabrics coated with organic solar cells have been developed, acting as energy source for charging a smartphone [9]. Surface coatings for windows in smartphones allowing an adaption of transparency and/or colour by applying a small voltage have also been developed. The main disadvantage of organic semiconductors consists in their significantly lower charge carrier mobility and conversion efficiency of organic semiconductors than achieved for inorganic semiconductors. A comparison with the current efficiency of organic solar cells to the efficiency of natural photosynthetic processes demonstrates that there is plenty of room for

improvement of the performance of synthetic organic semiconductors. For example, improvement is expected when organic molecules are perfectly ordered like in single crystalline domains. However, despite considerable efforts and progress in the field, structure-property relationships are often explored in a trial-and-error approach. Accordingly, no fundamental concepts have been developed which relate chemical structure and macroscopic properties. The main difficulty is caused by the complexity introduced by the large number of combinations of chemical building blocks, which impedes simple relations and the interplay between the solvent and the substrate. Controlling local structure on the nano- and microscale is often much easier than over large distances. Consequently, the resulting macroscopic properties may be affected by a variety of different structural elements across multiple length-scales. Accordingly, the fabrication of devices with a high performance suitable for various purposes remains difficult, because even minor changes in chemical structure may have a drastic impact on macroscopic properties.

A typical step in building organic field effect transistors (OFETs) relates to spin-coating or drop-casting a film from a solution of the organic material onto a (doped) silicon wafer with a thick oxide layer. The substrate can be used directly as the gate contact in a "bottom gate top contact" device. However, often organic molecules do not wet silicon wafers with an oxide layer, and thus crystalline layers of these molecules tend to dewet the substrate as soon as the temperature reaches values above their melting temperature. Due to their low viscosity, dewetting of small molecules can be a rather rapid process. Dewetting transforms a previously homogeneous film into an array of droplets or pancakes. Mostly, at the end of dewetting, no molecules remain in between the droplets, significantly hampering the formation of large-scale crystalline structures, which are a requirement for high-performance devices. Thus, the study of crystallization processes within dewetted thin films of organic molecules may allow identifying strategies for optimizing crystalline structures [10].

The here studied molecule belongs to a family of similar oligomers with a 2,5-dialkoxy-phenylene-bisthienylene monomer unit based on two thiophene (T) rings connected to a benzene ring (B),

3

abbreviated as TBT [11]. To enhance solubility in organic solvents and to allow for electrical decoupling of individual self-organized molecular wires, side-chains were added to the benzene ring. A wide range of molecules differing in the number of connected monomers and the chemical nature of the side-chains were synthesized [11]. In this study, we used 2-ethyl-hexane sidechains with five TBT groups, abbreviated as 5TBT. The detailed chemical formula of 5TBT is given figure 1A and figure S1 in the supporting information. The rather short stiff 5TBT was chosen as for longer molecules the crystallization rate decreases with the number of connected monomers [12, 13]. Based on the chemical structure, we anticipated that crystal growth along the π-π stacking direction [13] to be significantly faster than in the other directions. For example, due to the weaker interactions between side-chains crystal growth along the direction of the side-chains is expected to be much slower. 5TBT molecules are terminated by thiophenes at the ends, allowing for strong interactions with neighbouring molecules, as has been shown by Shokri et al [14]. In full agreement with these expectations, thin needle-like crystals of 3TBT (consisting of three TBT monomers) have been grown in solution [15]. However, spin coated thin films of 3TBT on silicon wafers were found to be highly unstable and rapidly dewetted. Using side-branched 5TBT, we hoped to find experimental conditions for the growth of stable films consisting of ultra-thin self-organized layers. For highly ordered molecules, we expected to obtain high intra-molecular conductivity along the backbone of the conjugated molecules. Based on a head to tail arrangement involving $\pi-\pi$ stacking of the thiophene rings at the end of the 5TBT molecules [14], we also anticipated that such inter-molecular couplings could allow for high conductivity in the direction of the backbone of the molecules of distances longer than the molecules. In highly ordered single-crystal-like arrangement of the molecules, high conductivity may also occur in the direction perpendicular to the long axis of the molecules, as was observed for single crystals of 8-hexyl-thiophene $(3HT)_8$ [16].

In this paper, we discuss a novel approach allowing the growth of large-scale crystalline structures consisting of uniquely oriented 5TBT molecules even from an array of droplets resulting from dewetting.

Based on these large-scale crystalline structures we fabricated FETs, which showed holes mobilities that were two orders of magnitude higher compared to non-crystallized films.

2. Experiments and Crystal Growth Mechanism

The 5TBT compound was synthesized by a palladium (0) Stille cross-coupling between the 2,5-diiodinated 3TBT (1) and two molar equivalents of the mono-stannylated 1TBT moiety (2). 1TBT, (2) and 3TBT were previously elaborated according to the literature [12] (Fig. S1). Each prepared compound was isolated by multiple flash chromatography sequences and fully characterized (see the supporting information for details of the synthesis). Fully stretched, a single molecule of side-branched 5TBT has a contour length of about 6 nm (see fig. 1A). The side chains can span a maximum distance of about 2 nm. In our experiments, 5TBT molecules were dissolved in toluene at room temperature to obtain a solution concentration of 0.02 mg/ml. We spin coated this solution onto Si wafers with a thermal oxide layer (thickness of $\approx$ 200 nm) at a spinning speed of 2000 rounds per minute (rpm), yielding a thin and homogeneous film with a thickness controlled by the spinning speed. We chose a value of 2000 rpm to reach a film thickness of $\approx$ 10 nm. Samples were heated on a Linkam hot stage, allowing simultaneous observation by optical microscopy, allowing a direct observation and determination of the film melting point (T_M), which was founded to be at 186 °C. When heating films of 5TBT to temperatures $T \geq T_M = $ 186°C, films dewetted spontaneously, forming shallow droplets with a size of about 2μm in width and a height of $\approx$ 40 nm. In agreement with the theoretical prediction by Seemann et al. [10], we observed that similar films did not dewet on silicon wafers, which were covered by a thin native oxide layer of only $\approx$ 2 nm. After melting, the temperature was cooled down to a lower crystallization temperature (T_{cryst}) and held there until the whole film was crystalline. Depending on the nucleation density and the crystal growth rate, which depended on T_{cryst} and film thickness, crystal growth lasted between 1 and 48 hours. Dewetting set in as soon as the molecules were in a mobile (e.g., liquid) state, i.e., above the melting

temperature. Unfortunately, we have not been able to follow the dewetting process in detail. The whole transition from the initially smooth film (after spin-coating, the surface roughness of the resulting thin films was less than ca. 1 nm, i.e. below the size of one molecule) to the final array of small droplets took less than one second once the temperature reached a value higher than the melting point. The most important consequence of the resulting pattern of droplets sitting on a dry substrate was the reduction of the nucleation probability. The nucleation rate scales with the volume of the crystallizable domain (in our case, this is the volume of an individual droplet) as has been impressively shown, for example by Massa and Dalnoki-Veress [17]. Indeed, for high crystallization temperature, a nucleus formed in only very few of the droplets. A low density of nucleation centers allowed for the growth of large crystalline domains consisting of molecules that all had the same orientation.

In order to check for a possible degradation of molecules at temperatures above 186 °C, we have performed a thermogravimetric analysis (TGA) which revealed that degradation of the molecule occurred at temperatures beyond ca. 325 °C (see figure S2 in the supplementary information). This observation strongly supported our conclusion that the change in topography observed at 186 °C was due to a mass-conserving dewetting process and not due to (local) degradation of molecules. However, we cannot exclude that due to interactions with the substrate, the transition was not from a crystalline state to a homogenous melt. Some state of liquid-crystalline order might have been reached, which, however, requires a high molecular mobility in order to allow for the observed very fast topographical transition caused by dewetting. In addition, surface freezing or pre-freezing even at temperatures above the melting point may be possible [18]. In [18], similar to our study, melting of the films was also accompanied by a dewetting process.

By varying crystallization temperature and film thickness, we were able to find experimental conditions that allowed growing single-crystal-like domains from liquid droplets that were substantially larger than the initial droplets. Optical microscopy images under crossed polarizer showed that all molecules within these crystalline domains had the same orientation (see figure 1B).

At a high T_{cryst} of about 170 °C, the formation of droplets with a small contact angle (i.e., their lateral dimension was much larger than their height) has only minor influence on crystallization. At such high T_{cryst} and the correspondingly slow crystal growth rates, molecules had a sufficient time to diffuse over long distances compared to the lateral size of a typical droplet. For $T_{cryst} \approx 160$ °C, crystals started to grow from a first droplet (nucleation site) and eventually became large enough to reach and include liquid molecules from surrounding droplets. Figure 1C visualizes the anticipated growth process in a cartoon. Once a nucleus is formed, crystals grow rapidly along the π- π stacking direction, which is parallel to the substrate, without significant growth in the vertical direction. Thus, the growing crystal is always covered by a reservoir of molten molecules, which can diffuse towards the growth front. Molecules from neighbouring droplets may also diffuse across the silicon surface, feeding the crystalline layers until their lateral size allows getting in contact with neighbouring droplets. There, crystal growth may accelerate as the number density of molecules close to the growth front is significantly higher. This process is repeated for other nearby droplets as many times as necessary for crystallizing all droplets. This repeated process was initiated by a single nucleus only and never interrupted through all the repetitions. Thus, the orientation of the initial nucleus was transferred to all involved molecules within the resulting domain, i.e., this growth process created large single-crystal-like domains with unique orientation of all molecules over hundreds of μm. In figure 1, we show optical micrographs taken under crossed polarisers for a sample grown at 160 °C. When the polarizer was oriented along or orthogonal to the fast growth axis of the crystal, which was along the diagonal from the bottom left to the top right corner of the micrograph, no light was detected (light was blocked by the analyser). However, when the polarizer was oriented at an angle of 45°with respect to the fast crystal growth direction, clear birefringence was detected, some light passed through the sample. The birefringence intensity was significant only for the crystalline droplets because the very thin crystalline layers in between the droplets contained much less molecules. However, when rotating the sample with respect to the polarizer, birefringence intensity increased or

decreased synchronously for all droplets within a single domain. This result confirms that all molecules within all crystalline layers in all droplets were oriented in a unique way.

Upon reducing T_{cryst}, the nucleation density increased, and thus the size of crystalline domains of unique molecular orientation decreased. Upon quenching the molten sample to room temperature (e.g., by taking the sample off the hot stage), the nucleation density became so high that each droplet contained at least one nucleus. Thus, no correlations in orientation between neighbouring crystalline droplets were observed. In addition, crystal growth became so fast that the comparatively slow diffusion did not allow for any significant change in shape of the crystallized droplets. Already for $T_{cryst} < 140$ °C, each droplet contained at least one nucleus. Lowering the nucleation density by increasing T_{cryst} allowed forming larger crystalline domains, as shown in figure 2. For $T_{cryst} = 164$ °C, growing crystalline domains starting from various nuclei eventually coalesced and formed an array of polygons of a typical size of approximately 200 µm. In figure 2, the domain borders were highlighted by red lines. For the lower nucleation density established for $T_{cryst} = 176$ °C domains with a size up to millimetres were found. At $T_{cryst} = 176$ °C, differences in growth speed between the π-π stacking direction and the perpendicular direction were smaller than for $T_{cryst} = 164$ °C. In addition, surface diffusion of 5TBT became faster than the lateral growth, introducing zones depleted from molecules between the crystals (see figure 2B). At $T_{cryst} > 176$ °C (images not shown here), crystalline domains showed elongated shapes and grew in length and height, but not significantly in width. Under these conditions, large depleted zones formed and the crystals obtained a needle-like shape. In summary, in spite of dewetting of the molten film on silicon wafers with thermal oxide layers, large domains of ultra-thin crystalline layers with unique molecular orientation were formed at $T_{cryst} = 164$ °C. Derived from a low nucleation density, these domains extended over thousands of droplets, covering areas of up to ≈ 0.2 mm^2.

3. Atomic Force Microscopy Characterization

For the case of large domains of ultra-thin crystalline layers obtained at T_{cryst} = 164 °C, we acquired detailed information about the orientation of the molecules within individual crystalline layers by AFM (see figure 3). The profile of figure 3B shows steps with a height in multiples of 2 nm, a value comparable with the characteristic width of 5TBT (figure 3C). Since the molecule is rather stiff, it can be approximated by a cuboid with a width of about 2 nm and a length of about 6 nm. The existence of crystals with a thickness of 4 nm (i.e., less than the maximum length of 5TBT) suggests that the molecules were not oriented with their backbone in the direction normal to the substrate. Furthermore, recurring steps with a height of 2 nm within the stacks of crystalline layers compares well with the maximum span of the side chains, suggesting an edge-on orientation of the molecules. As no individual layers of a thickness of only 2 nm were found on the substrate, we tentatively conclude that only bilayers could form on the substrate, probably due to explicit interactions between the side chains. This orientation of the backbone of the molecules parallel to the substrate is consistent with the observation of large dipole moments along the fast growth direction, supporting our assumption of π- π stacking along this direction. In the topographical AFM images shown in figure 3 and in figure 4, we observed an intriguing surface pattern, forming small domains in a quasi-checkerboard pattern. Unlike a true checkerboard, the characteristic features of the pattern were neither quadratic nor perfectly regular. Two distinctly different sub-patterns were observed, each consisting parallel lines. However, the orientation of these groups of lines exhibited an angle of (80 ± 2)° between them. The AFM image shown in figure 4 was taken with the slow scanning direction of the AFM approximately in the direction of the axis of the dipole moment, which was deduced from optical micrographs taken under crossed polarisers. The axis of the dipole moment indicated by a green arrow coincided rather well with the bisectrix of the two orientations of the patterns observed by AFM. Interestingly, while the line pattern, i.e. the angle between the two orientations, did not change much, the distance between individual lines varied strongly with the thickness of the corresponding crystalline region, ranging from ≈ 25 nm up to ≈ 180 nm. Intriguingly,

the average lateral size of the domains also increased with crystal thickness, yielding an approximately constant number of *ca.* 10 parallel lines per domain, independent of the thickness of the crystalline region. The same surface pattern with an angle of $(80 \pm 2)°$ between groups of lines was observed for crystals grown on silicon wafers with very thin native oxide layers of ca. 2 nm, where 5TBT did not show any signs of dewetting. For such substrates, we obtained homogeneous films, which allowed for rather precise measurements of film thickness, the step heights and the distances between lines. Preparing films of thicknesses ranging from 4 nm (double layer) up to 40 nm by varying the spinning speed allowed determining the distance between the lines for increasing thickness of the crystalline domains. A linear dependence was found as can be seen in figure 5.

We performed an X-ray diffraction experiment on a several μm thick film of 5TBT on a silicon substrate. The analysis of the corresponding results (see Supporting Information, Figure S3) allowed us to deduce characteristic parameters of a possible crystal unit cell. The sample was prepared by repeatedly drop-casting a highly concentrated solution of 5TBT in toluene onto the substrate, followed by a drying step. During drying, the molecules formed randomly oriented small crystallites within the thick film. X-ray diffraction pattern showed several strong peaks (see Supporting Information, Figure S3) which we attributed to scattering from (1 0 0), (0 1 0) and (0 0 1) faces of the crystal structure. Several smaller peaks were attributed to e.g. scattering from (1 1 0), (1, 2, 0) and (3, 0, 1) faces, assuming an angle $\gamma = 107°$ between the (1 0 0) and (0 1 0) faces. We compared the obtained unit cell parameters with characteristic distances within the molecules. The value of a = 1.4 nm can be related to the distance between stacked side chains. This value suggests a slight interdigitation between sidechains, it is slightly lower than the step height of about 2 nm observed by AFM. The unit cell parameter b = 1.3 nm compares favourably with the size of a single TBT monomer unit. The unit cell parameter c = 0.34 nm strongly supports our suggestion of π-π-stacking between 5TBT molecules. Indeed, an absorption study exhibits the pi-stacking existence between 5TBT conjugated segments. The absorption maximum in the solid state (487 nm) is red-shifted of 17 nm and compared to the one of the 5TBT solution in CHCl3 (10-5M)

(470 nm) (See Figure S4 of the UV-Vis spectra of 5TBT in solution and in the solid state). This is the signature of an enhanced conjugation in the solid state compared to the solution, due to the π-stacking between the conjugated segments despite of the presence of the substituting alkoxyle solubilizing side chains beared by each 5TBT molecular entity. Additionally, more elaborate X-ray diffraction experiments, e.g. on single crystals of 5TBT, may allow a more detailed analysis of all parameters of the unit cell.

The molecular orientation of 5TBT within the layers in the thin film crystallized from the molten state could be deduced from the microscopy investigations. Several ways of stacking of 5TBT molecules may be possible: Benzene rings may stack on benzene rings or thiophene rings may stack on thiophene rings. Alternatively, we also consider that thiophene rings stack on benzene rings or vice versa. As the backbone consists of a repeat sequence of two thiophene rings and one benzene ring, the possibilities for thiophene stacking are larger. Using the theoretically predicted π-π stacking distance for thiophene with benzene of ≈ 0.5 nm [19], this would result in an angle of ≈ ±45°, which is surprisingly close to the observed angle of *ca.* 40° with respect to the fast growth axis. In order to clarify if the surface structure is induced by π-π interactions or caused by surface stresses during the crystallization process further investigations are needed. We suppose, for example, that annealing in vapour of toluene or dodecane may allow relaxing surface stresses, helping to identify the origin of the observed surface pattern.

4. Field Effect Transistor Measurements

We fabricated first FET prototypes from large-scale crystalline domains grown after dewetting. Silicon wafers were cleaned in baths of soapy water, acetone and isopropanol for 15 min each. Subsequently, the clean substrates were introduced into a glove box under nitrogen atmosphere, where spin coating and

crystal growth experiments were performed in analogy to the experiments described above. By evaporating an injection layer (a few nm thin molybdenum oxide) and subsequently silver contacts (20 nm) through a mask, we established a "top contact bottom gate" FET. Contacts were evaporated in a high vacuum chamber connected to the glove box. Characterization was performed under nitrogen atmosphere in the glove box. The transistor channel length is 21,9 mm and its width is 60µm. Charge carrier mobility is expected to be different along various axis of the organic semiconducting crystals. We anticipated a higher mobility along the π-π stacking direction [16]. Unfortunately, the size of the crystalline domains grown at 164 °C was less than the length of the FET channel. Therefore, the resulting average values of mobility reflected transport across multiple randomly oriented crystalline domains within the channel (see figure 2A).

Output and transfer characteristics of the obtained FETs are shown in figure 6. All devices showed low leakage, reasonably low contact resistance and well reproducible characteristics. The output characteristic (figure 6A) was typical for an OFET device. Here, the organic semiconductor and the gate can be seen as a capacitor with the silicon oxide as dielectric. By applying a voltage V_{SD} between source and drain, charge carriers can be extracted through the drain contact. For $|V_{DS}| \ll |V_{GS}|$, the accumulation layer connected both contacts, resulting in an Ohmic behaviour, called the linear regime for the extracted charge carriers as a function of V_{SD}. For large values of V_{SD}, the region close to the drain became depleted from charge carriers, resulting in a space charge limited current (SCLC) across the depleted region. When increasing V_{SD} further, the depleted region grew and the SCLC had to bridge a larger gap, which effectively limited the maximum current, called the saturation regime shown in Figure 6A for the current I_{SD} between source and drain as a function of V_{SD}. In the saturation regime with holes as majority charge carriers, the mobility can be extracted using following equation [20]:

$$\mu = \frac{2L}{WC}\left(\frac{d\sqrt{|I|_{DS}}}{dV_G}\right)^2$$

where L denotes the length of the channel (the distance between source and drain electrodes), W the width of the channel (the length of the electrodes), and C the capacity of the dielectric material between gate and semiconductor. We take $C \approx 15$ nF/cm^2 for a 200 nm thick silicon oxide layer.

For the tested samples, the values of the extracted hole mobility ranged from 1.7 to 4.5×10^{-4} cm^2/Vs. Small differences between samples are expected for the following reasons: in the setup of the OFETs, the orientation of the crystalline domains was not controlled and the evaporation of injection layer and silver contacts did not yield always the same contact resistance. Re-measuring the mobility after an exposure to air for one month yielded values which were only about 10% lower than the initially measured values indicating that the devices were highly stable even in air. Tentatively, we attribute this high stability to the rather low HOMO level of about -4.7eV.

As a reference, we prepared also OFETs from spin coated 5TBT films without controlled crystallization treatment. In this case, the values of the charge carrier mobility were of the order of 10^{-6} cm^2/Vs, in accordance with the result of a previous study on spin coated 4TBT thin films [21]. Thus, highly disordered thin 5TBT films showed a by two orders of magnitude reduced mobility, supporting the hypothesis that charge transport in systems exhibiting π- π stacking is enhanced by molecular order. Much higher mobility values have been reported in the literature. For example, Sirringhaus et al. [22] found a FET mobility of up to 0.1 cm^{2}V^{-1}s^{-1} for a conjugated polymer. However, Crossland et al. [23] showed that an ensemble of crystalline domains having differently oriented crystal unit cells and grain boundaries between these domains can decrease the mobility easily by two orders of magnitude.

5. Conclusion.

Although films of liquid 5TBT dewetted on silicon wafers with thermal oxide layers, we were able to grow large-scale 5TBT crystalline domains with unique molecular order. These crystalline domains were

implemented in field effect transistor devices that showed high stability in ambient air. Growth of crystalline domains was governed by strong interactions in the π-π stacking direction and by much weaker interactions in the orthogonal directions. We anticipate that our approach can be applied for a wide range of organic semiconductors with similar asymmetric growth properties, common for molecules exhibiting π-π stacking and having appropriate side chains.

References:

[1] D. Woehrle, D. Meissner, Advanced Materials 3 (1991) 129-138.

[2] S. Günes, H. Neugebauer, N. S. Sariciftci, Chemical Reviews 107 (4) (2007) 1324-1338.

[3] S. Khan, L. Lorenzelli, R. Dahiya, IEEE Sensors Journal 15 (6) (2014) 3164-3185.

[4] P. Zhao, Y. Wu, Ch. Feng, L. Wang, Y. Ding, A. Hu, Analytical chemistry 90 (7) (2018) 4815–4822.

[5] Ch. Fenzl, Th. Hirsch, Otto S. Wolfbeis, Angewandte Chemie International Edition 53 (13) (2014) 3318-3335.

[6] X. Gu, Y. Zhou, K. Gu, T. Kurosawa, Y. Guo, Y. Li, H. Lin, B.C. Schroeder, H. Yan, F. Molina-Lopez, Advanced Energy Materials 7 (14) (2017) 1602742.

[7] S. Holliday, J. E. Donaghey, I. McCulloch, Chem. Mater. 26 (1) (2014) 647-663.

[8] V. Skrypnychuk, G.-J. AH Wetzelaer, P. I. Gordiichuk, S. CB Mannsfeld, A. Herrmann, M. F Toney, D. R Barbero, Advanced Materials 28 (12) (2016) 2359-2366.

[9] X.-Sh. Zhang, M. Han, B. Kim, J.-F. Bao, J. Brugger, H. Zhang, Nano Energy 47 (2018) 410-42.

[10] R. Seemann, S. Herminghaus, K. Jacobs, Physical Review Letters 86 (24) (2001) 5534.

[11] J. C. Flores, J. P. Lère-Porte, F. Serein-Spirau, J. J. E. Moreau, K. Miqueu, J. M. Sotiropoulos, P. Baylere, M. Tillard, C. Bellin, Eur. J. Org. Chem. 2007, 4019-4031.

[12] M. N. Nair, N. Hobeika, F. Calard, J.P. Malval, S. Aloïse, A. Spangenberg, L. Simon, M. Cranney, F. Vonau, D. Aubel, F. Serein-Spirau, J.-P. Lère-Porte, M.-A. Lacour, T. Jarrosson, Physical Chemistry Chemical Physics 16 (25) (2014) 12826-12837.

[13] G. Reiter, G. Strobl, Progress in understanding of polymer crystallization, Book volume 714 (2007) Springer Verlag.

[14] R. Shokri, M. A. Lacour, Th. Jarrosson, J. P. Lère-Porte, F. Serein-Spirau, K. Miqueu, J. M. Sotiropoulos, F. Vonau, D. Aubel, M. Cranney, G. Reiter, L. Simon, Journal of the American Chemical Society 135 (15) (2013) 5693-5698.

[15] S. Motamen, Ch. Schörner, D. Raithel, J. P. Malval, Th. Jarrosson, F. Serein-Spirau, L. Simon, R. Hildner, G. Reiter, Physical Chemistry Chemical Physics 19 (24) (2017) 15980-15987.

[16] W. Hourani, K. Rahimi, I. Botiz, F. P. V. Koch, G. Reiter, P. Lienerth, Th. Heiser, J. L. Bubendorff, L. Simon, Nanoscale 6 (2014) 4774.

[17] M. V. Massa, K. Dalnoki-Veress, Phys. Rev. Lett., 92 (2004) 255509.

[18] M. Tariq, O. Dolynchuk, T. Thurn-Albrecht, Macromolecules, 52 (2019) 9140–9148.

[19] O. Castellano, R. Gimon, H. Soscun, Energy and fuels 25 (6) (2011) 2526-2541.

[20] P. B. Shea, J. Kanicki, Journal of Applied Physics, 98 (2005) 014503.

[21] P. Lienerth, *Elaboration and characterization of field-effect transistors based on organic molecular wires for chemical sensing applications*, PhD Thesis, University of Strasbourg (2014).

[22] H. Sirringhaus, N. Tessler, R. H. Friend, Science, 280 (1998) 1741-1744.

[23] E. J. W. Crossland, K. Tremel, F. Fischer, K. Rahimi, G. Reiter, U. Steiner, S. Ludwigs, Adv. Mater.,

24 (2012) 839-844.

Figure captions

Figure 1: A) Molecular structure of 5TBT with the indication of its characteristics lengths.

B) Two optical micrograph of the same region taken under crossed polarizer before and after rotation of the sample by 45 °. The orientation of the polarizers with respect to the orientation of the sample is indicated by the red crosses. For the whole image, the birefringence intensity changed with orientation of the sample with respect to the polarizers, demonstrating that the orientation of all molecules within all droplets was the same, a correlation generated through the crystallization process.

C) Sketch of the growth process which allowed correlating the orientation of 5TBT molecules across many droplets generated by a dewetting process: (i) At relatively high crystallisation temperatures, crystallisation can be started by the formation of a nucleus in one droplet only, as the nucleation probability is extremely low. (ii) Driven by anisotropic growth only one crystalline layer grows until its size reaches the boundary of the droplet, which represents the reservoir of crystallisable molecules. At this stage, many molecules within the droplet are still liquid. (iii) This first layer is growing beyond the boundaries of the droplet, fed by molecules from within the droplet but also by molecules from neighbouring droplets, which diffuse towards the crystalline layer. When the size of the crystalline becomes large enough to get in contact with neighbouring droplets it will act as a seed and initiate crystallisation in these droplets. (iv) Repetition of steps (ii) and (iii) will propagate crystallization across many droplets. As growth is never interrupted and no additional nucleation event take place due to the low nucleation probability, all molecules within the whole crystalline structure have the same orientation.

Figure 2: Large-scale images of crystalline domains grown at (A) 164°C and (B) 172°C, respectively. Red lines indicate the borders between domains resulting from different nuclei. The domains size depends on the distance between nuclei: the lower the crystallization temperature, the higher the nucleation density. As a consequence of different growth velocities along the π-π stacking direction and in the orthogonal directions, empty (depleted) zones without crystalline structure are visible in (B). At

high crystallization temperatures, the crystal growth rate becomes similar to the rate of diffusion. Due to the large size of the observed region, the images were stitched together using several independently taken optical micrographs.

Figure 3: (A) AFM topography image (3 μm x 3 μm) and (B) the corresponding height profile from a sample grown at 164°C.

Figure 4: A larger-scale AFM topography image (10 μm x 10 μm) on a sample grown at 164°C. The inset shows a zoom to the indicated 1×1 μm^2 region. The green arrow indicates the direction of the large dipole moment as determined by optical microscopy under crossed polarisers. Represented by differences in height, the positions of the initial droplets still can be identified in this large-scale image. In the zoomed image, a surface pattern can be seen clearly, consisting of lines oriented at angles of ± 40° with respect to the axis of the dipole moment.

Figure 5: Plot of the distances measured between adjacent lines of the surface patterns as a function of the thickness of the crystalline region. For obtaining these results, a series of films differing in thickness were prepared at different spinning speed on silicon wafers with a thin native oxide layer. Results are consistent with observations on crystals grown on silicon wafers with thicker thermal oxide layers.

Figure 6: Typical output and transfer characteristics of a 5TBT FET built as described: (A) Drain source current as a function of drain source voltage for different gate voltage as indicated in the legend. (B) Drain source current as a function of gate voltage at a drain source voltage of 10 V.
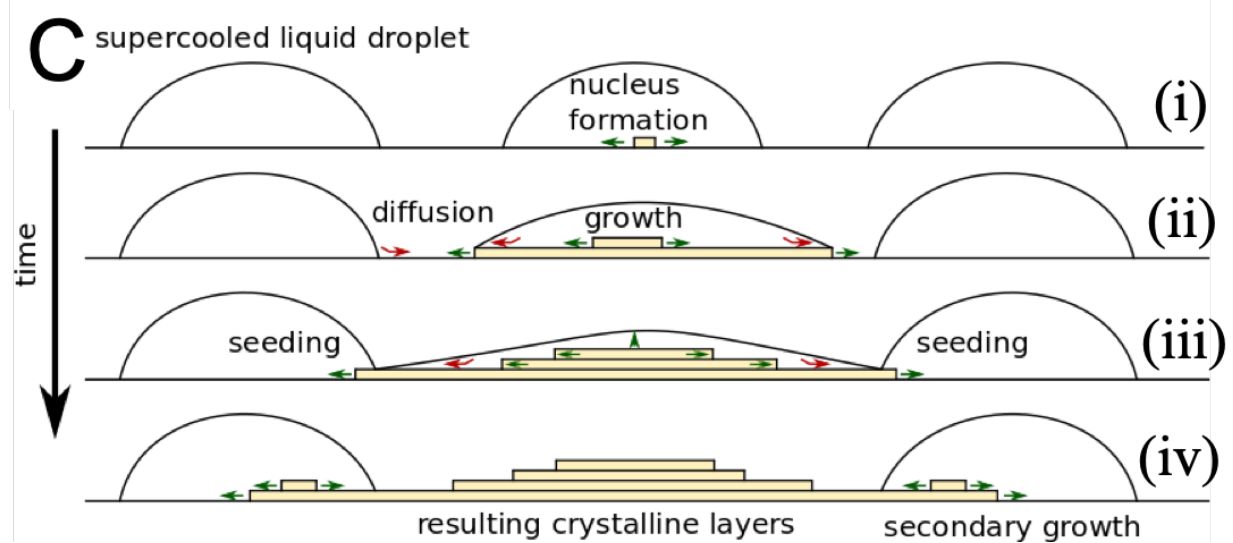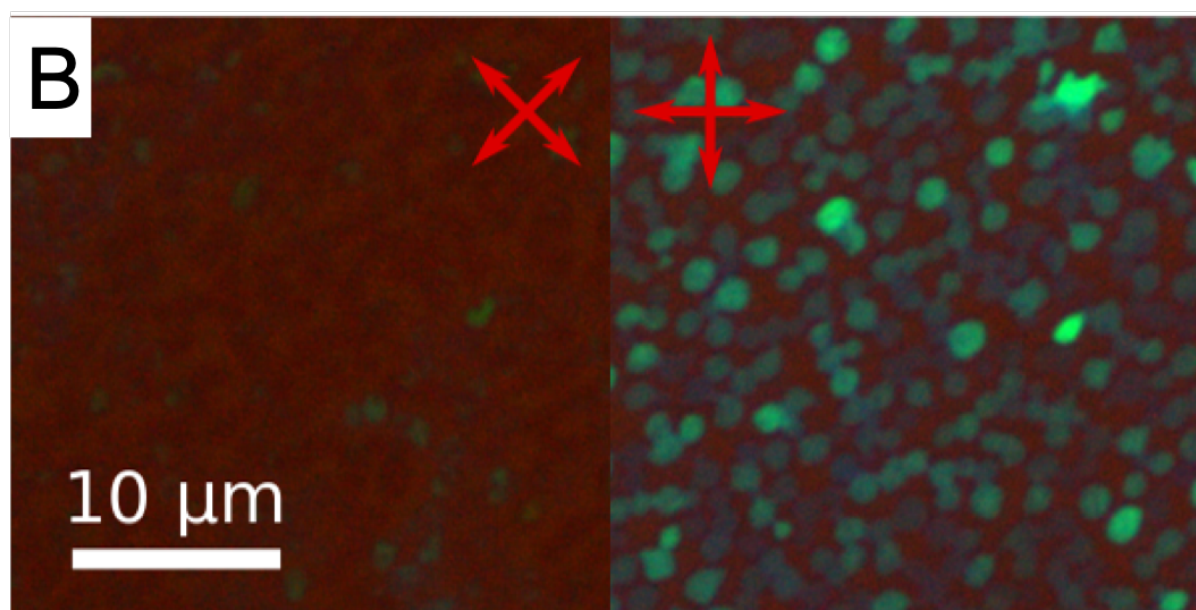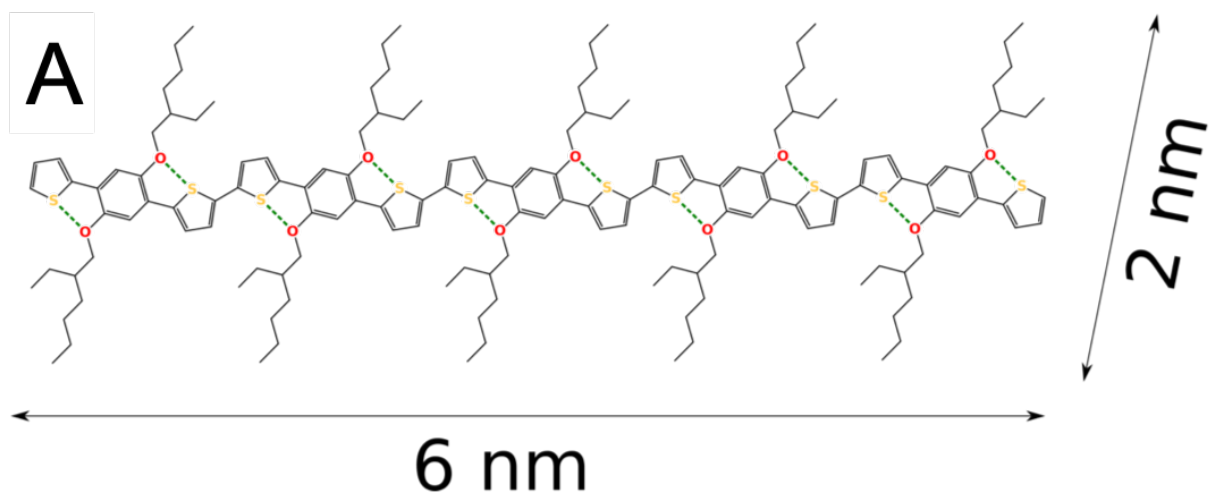
A

2 nm
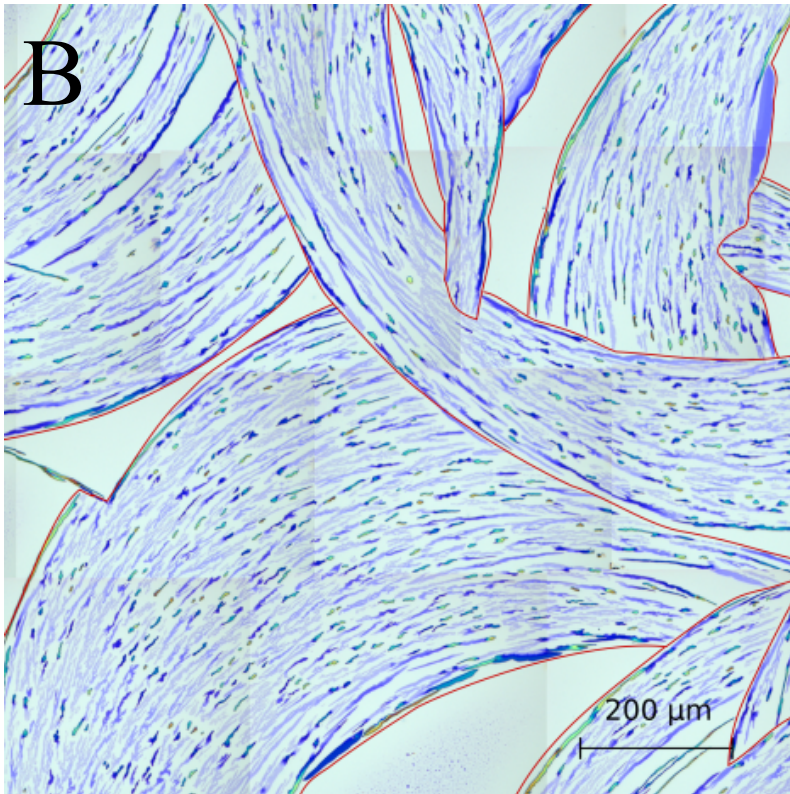
6 nm

B

10 µm

C supercooled liquid droplet

nucleus formation

(i)

time

diffusion growth

(ii)

seeding seeding

(iii)

resulting crystalline layers secondary growth

(iv)
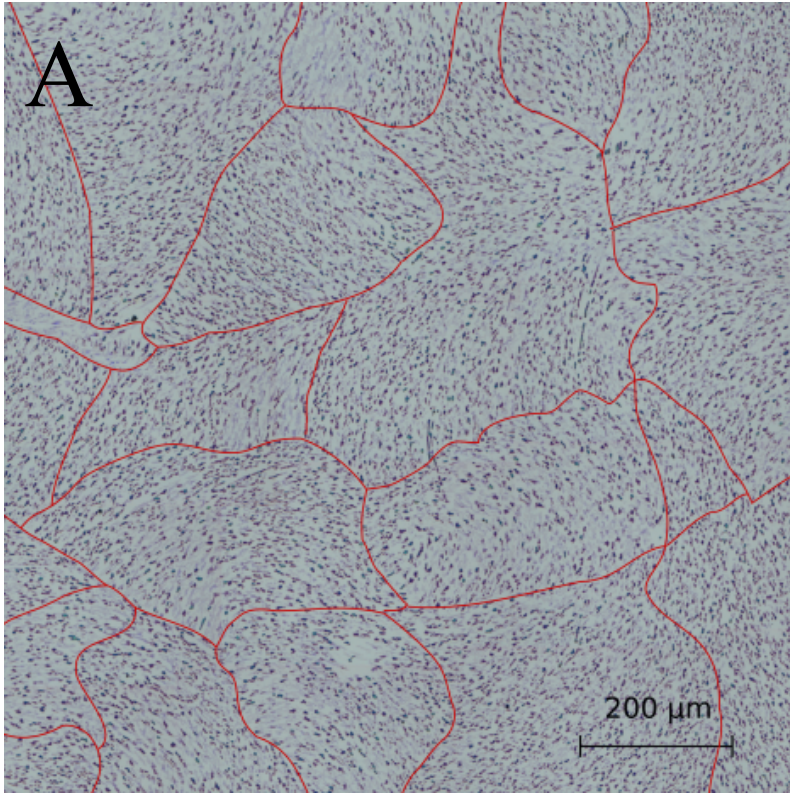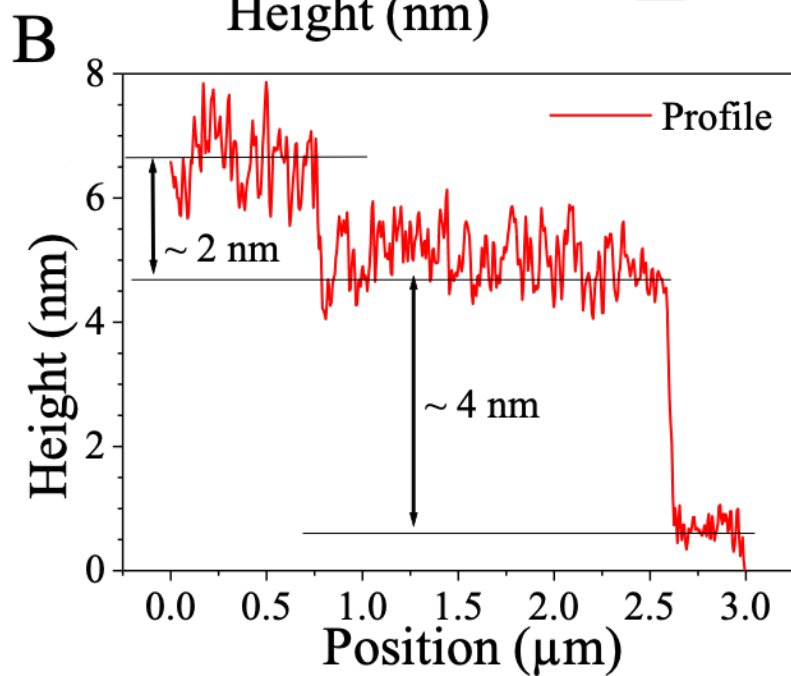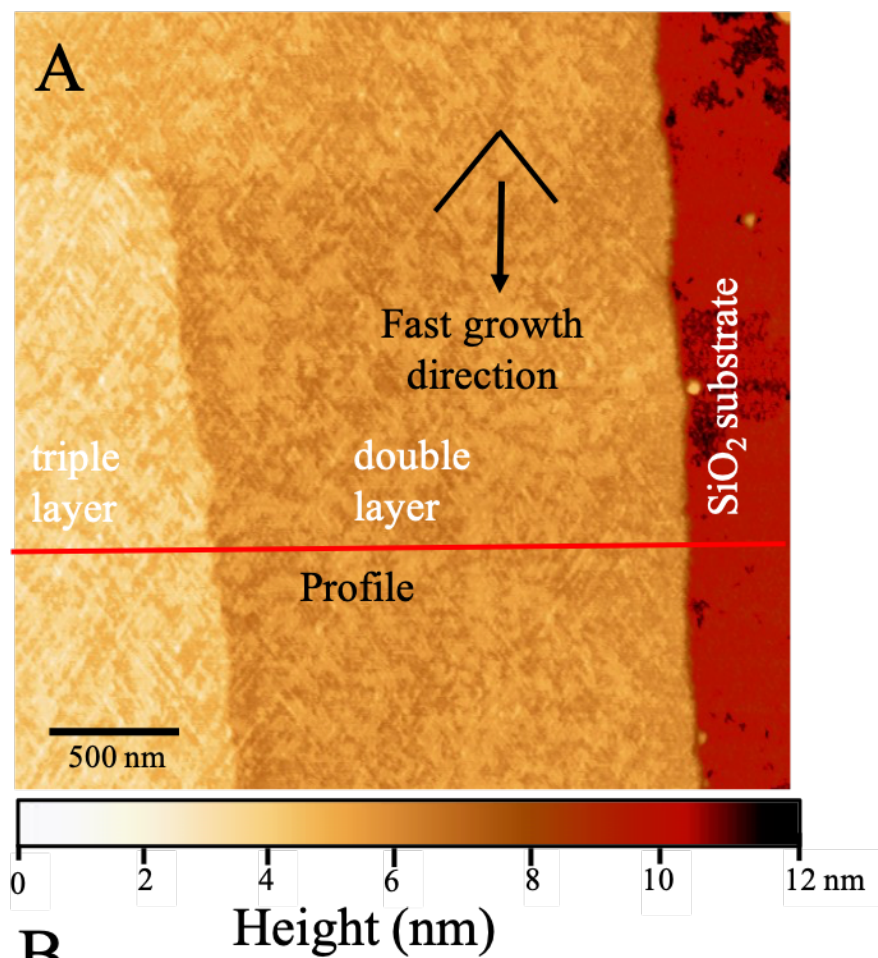
Figure 1

Figure 2

Figure 3
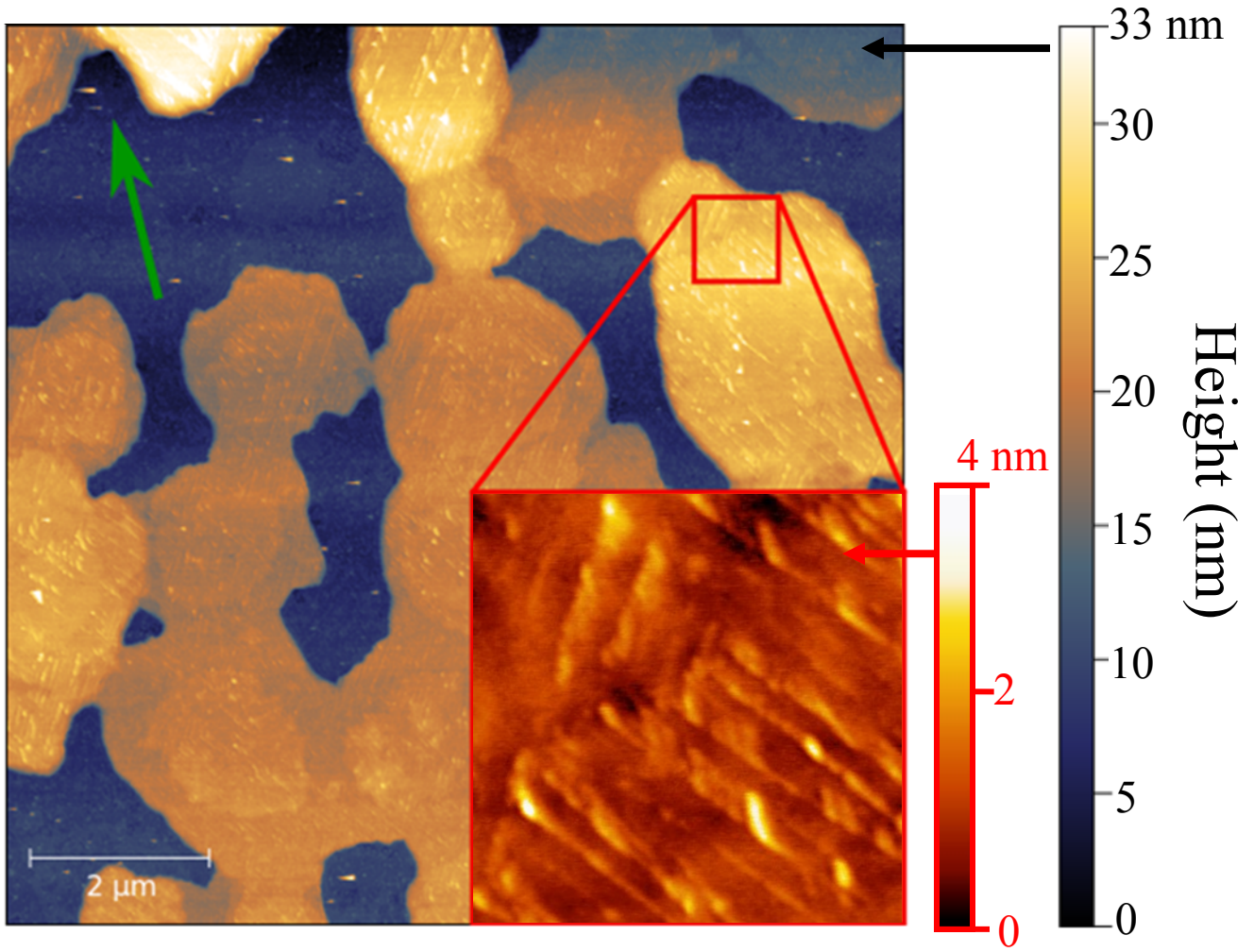
Figure 4

Figure 5

Figure 6